The role of NO_2 and NO in the mechanism of hydrocarbon degradation leading to carbonaceous deposits in engines

Radomir I. Slavchov[1,2*], Maurin Salamanca[2], Danilo Russo[2], Ibrahim Salama[3], Sebastian Mosbach[2], Stuart M. Clarke[3], Markus Kraft[2,4,5], Alexei A. Lapkin[2,5], Sorin V. Filip[6]

released: 18 December 2019

[1] School of Engineering and Materials Science
Department of Chemical Engineering
Queen Mary University of London
Mile End Road, London E1 4NS
United Kingdom
E-mail: r.slavchov@qmul.ac.uk

[2] Department of Chemical Engineering
University of Cambridge
West Site, Philippa Fawcett Drive
Cambridge, CB3 0AS
United Kingdom

[3] BP Institute,
University of Cambridge
Bullard Laboratories, Madingley Road
Cambridge, CB3 0EZ
United Kingdom

[4] School of Chemical and
Biomedical Engineering
Nanyang Technological University
62 Nanyang Drive
Singapore, 637459

[5] Cambridge Centre for Advanced
Research and Education
CREATE Tower
1 CREATE Way, 138602
Singapore

[6] BP Formulated Products Technology,
Research and Innovation
Technology Centre
Pangbourne
United Kingdom

Preprint No. 247

Keywords: Engine deposits, NO_x, autooxidation, gasoline, radical chain, anti-oxidant.

Edited by
Computational Modelling Group
Department of Chemical Engineering and Biotechnology
University of Cambridge
West Cambridge Site, Philippa Fawcett Drive
Cambridge, CB3 0AS
United Kingdom

Fax: + 44 (0) 1223 334796
E-mail: c4e@cam.ac.uk
World Wide Web: https://como.ceb.cam.ac.uk

Abstract

A hypothetical mechanism of degradation of the fuel droplet leaking out from the injector nozzle in a direct injection combustion engine has been proposed recently. This involves as a key step a radical chain oxidation initiated by NO_2 and branched by nitric oxide, NO, both produced by the combustion. The degradation causes the formation of injector nozzle carbonaceous deposits. The present work gives an experimental validation of some of the assumptions behind this model. An autoclave is used to oxidize isooctane under conditions relevant to the cylinder wall near the nozzle (~150 °C, 10 bar, 5% O_2, 100 *x*ppm of NO_2 and 500 *x*ppm NO in the gas phase), and the degradation products are monitored via gas chromatography-mass spectrometry (GC-MS). The results show that no fuel degradation is observed in the absence of NO_x. NO appears to be able to initiate a radical chain by producing NO_2. Nitric oxide also alters the radical chain by transforming the alkyl peroxy radicals to more reactive alkoxy radicals, resulting in a range of different products. In addition, NO tends to terminate the radical chain by neutralizing a fraction of the alkyl peroxy radicals, producing alkyl nitrates as termination products. The existence of a radical chain is supported by demonstrating antioxidative action of a radical scavenger. The chemical reaction mechanism is investigated, based on the detected products, and the key species involved in the degradation process are identified.

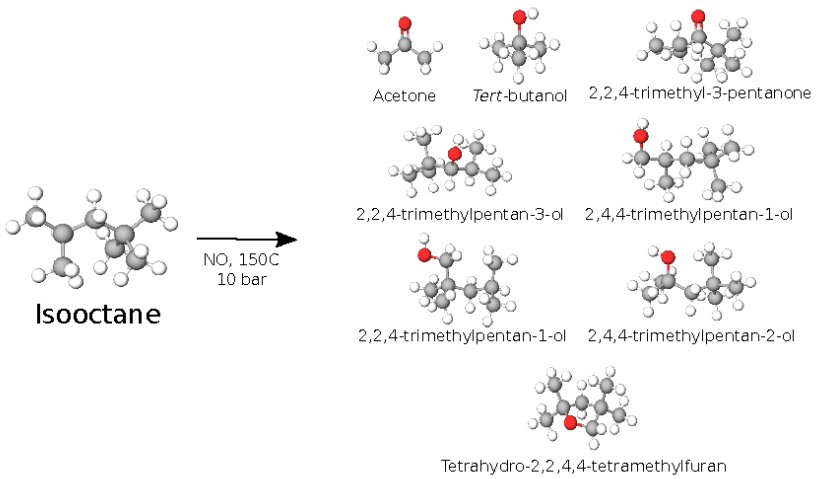

Highlights:

- Isooctane degradation is studied under conditions prevalent at engine cylinder wall.
- NO_2 initiates oxidation radical chain in impinged gasoline; >50 products identified.
- O_2 alone, in the absence of NO_x, does not produce significant liquid fuel degradation.
- If only NO_2 is present, the key reactive intermediates are alkylperoxy radicals.
- If both NO_x ($NO+NO_2$) are present, the key reactive intermediates are alkoxy radicals.

Contents

1. Introduction

In a direct injection engine, after the fuel injection, a pool of liquid fuel wets the surface around the nozzle at the cylinder head, due to fuel leakage through the seal after the injection [1-4] and residue from the fuel spray. This liquid fuel is exposed to high cylinder pressure (10–30 bar), elevated temperature (100–180 °C at the walls [5]), and to a gas quench layer containing approximately 5-10% oxygen, ~500 *x*ppm of nitric oxide, NO, and ~100 *x*ppm of NO_2 [4]. Under these conditions, the fuel degrades. Most likely, the initial stages of the injector fouling are dominated by the autooxidation of this fuel film. Later on, soot [3] and up to 10-50% lubricant-derived material [6,7] add to the produced sticky matter, reinforcing the deposit to produce a hard, porous material.

The injector deposits have detrimental effects on the engine operation, and are responsible for a long list of problems: they can triple soot emissions in gasoline direct injection engines, and increase NO_x emissions by as much as 40% [8]; the deposits insulate the engine wall causing its temperature to rise [4]; flaked deposits can produce engine "rumble" and knock, and the pores of the deposits can store fuel, especially its heavy components, and release it at an inappropriate stage of the cycle [9]. The prevention of the appearance and the removal of deposits is a serious issue for the automotive industry. The research in the degradation processes is further stimulated by (i) increasingly stringent emission standards and the resulting higher requirements for the spray characteristics; (ii) the search for possible renewable biofuel blends for gasoline (e.g., ethyl *tert*-butyl ether [10], and more exotic components [11]), which often result in decreased oxidative stability potentially leading to accumulation of harmful peroxides; (iii) the detrimental interaction of certain gasoline octane enhancers (such as the toxic N-methyl aniline [12]) with products of gasoline degradation, producing sludge and varnish [12,13].

The NO_x produced in the cylinder also causes degradation of the lubricant, and especially of the gasoline components that accumulate in the lubricant [14-21]. NO_x and gasoline are introduced into the lubricant first at the cylinder walls; further, both NO_x and degraded gasoline pass through the piston rings as blow-by, and cause extensive oxidation of the lubricant in the crankcase, initially producing deposits precursors [20], then resins, sludge and varnish [22]. If either NO_x or gasoline are absent, no varnish is produced [14]. This type of gasoline and NO_x-induced lubricant degradation produces piston deposits [14], turbocharger coking [21] and deposits in the lubricant pump.

Decades ago, the typical engine sludge and varnish would have contained significant amounts of N-containing products [14], which was the reason for intensive research on the role of NO_x in the degradation process. A number of *deposit precursors* (primary reaction products of hydrocarbons, NO_x and O_2) that contain nitrogen have been identified [23]: nitro-, nitrate and nitroso functionalities have been reported; some polyfunctional compounds such as 1-nitrate-2-alkanones and alkylhydroxylamines are often mentioned. In the 1980s, the so-called black sludge became a common problem at the cylinder head [22,24], and it did not appear to be rich in N. This seems to have resulted in the NO_x degradation mechanism dropping out of fashion. However, the absence of organic N does not mean that NO_x are not involved – particularly if they only initiate and lead to branching of the radical chain that oxidizes the gasoline, then no nitrogen will remain in the degradation products [4]. For example, no organic N-containing compounds were detected in the degraded lubricant in the tests done in Ref. [20], despite the fact that NO_x clearly contributed to the degradation.

The details of this degradation process are essential to understand the potential gasoline engine deposit problems, especially with the advance of direct injection spark ignition engines, which can be susceptible to injector nozzle deposits. Various fragmentary hypotheses have been proposed for the degradation mechanism, often questionable and contradictory. Colclough [23] claims that it is NO_2 rather than NO that causes the problem. On the other hand, the lubricant

test of Nakamura et al. [25] considered the degradation under the action of NO alone. Moreover, while NO is indeed the weaker initiator, it is more concentrated in the quench layer, and in addition has a branching effect that accelerates the autooxidation [4]. It is unclear to what extent the degradation occurs in the engine cylinder, the crankcase, and in the lubricant lines. Some bench tests for *lubricant* degradation may not be fully representative of the conditions in the quench layer next to the cylinder walls, as there the gas phase is a mixture of 5-15% of O_2 with the very potent radical chain initiator NO_2 and the branching agent NO – a test that misses one of these components is likely to produce deposit precursors different from those in the engine. Peroxides and hydroperoxides are considered to be major intermediates [22], but in the presence of NO, the oxidation might proceed through alcohols instead [4]. Both nitrogen oxides react with the reaction intermediates [18]. Ref. [21] assumes the nitrate esters are produced by reaction of NO_2 with alcohols that are produced from base oil hydrocarbons, but no reaction mechanism has been suggested. Very few tests and models of injector fouling in the literature consider NO_x as a factor driving the *fuel* degradation [4,26]; we are not aware of any experimental data published on NO_x-induced gasoline degradation. It is often the case that the studies of the oxidative degradation do not consider specific radical chain initiators at all, e.g., Ref. [27]. Even the most representative tests in the literature that consider all three essential components of the sludge formation, specifically fuel, NO_x and air [18,28,29], might still miss essential physicochemical factors such as the high cylinder pressure, that (i) increases the gas phase concentration of NO_x considerably, and (ii) allows the otherwise volatile gasoline components to remain in the liquid state and to undergo nitro-oxidation.

The main aim of this study is to design a bench test to investigate the initial stages of the degradation of gasoline fuel or gasoline components under conditions similar to those occurring at the engine cylinder wall: high pressure, temperature of the order of 150 °C, 5% O_2, with hundreds of ppm of NO_2 and NO each. In accordance with the short review above, several experiments were carried out to assess the role of NO_2, NO and O_2 in the degradation process, and to identify the main primary degradation products (the deposit precursors) that form under engine conditions, and the chemical reactions that lead to them.

2. Method and materials

Materials. NO and NO_2 balanced with N_2 were supplied by BOC in custom-made 1.5 L cylinders. Three such NO_x-cylinders were used: (i) 1000 *x*ppm NO; (ii) 200 *x*ppm NO_2; and (iii) a mixture of 1000 *x*ppm NO and 200 *x*ppm NO_2. Anhydrous isooctane (99.8%) was purchased from Sigma-Aldrich, and purified by percolation through a packed column containing 100 g of silica gel and 100 g of basic activated alumina under Ar atmosphere. Prior to use, silica gel and alumina were heated in advance for 12 h at 300 °C, as detailed in Ref. [30]. The radical scavenger (2,2,6,6-tetramethylpiperidin-1-yl)oxyl (TEMPO) and the analytical standards for the calibration of acetone and methylpropan-2-ol for gas chromatography-mass spectrometry (GC-MS) were purchased from Sigma-Aldrich and used as received. The 2,4,4-trimethylpentan-2-ol standard was from TCI, and used as received.

Reactor. The reaction system has been described previously in Ref. [30], and is shown schematically in Figure 1. Briefly, the 150 mL stainless steel reactor is a batch apparatus with respect to liquid, with continuous bubbling of gas through the liquid phase. The autoclave was purchased from HEL Ltd. The liquid isooctane (60 mL for each run) was added to a glass insert fitted in the autoclave. The reactor was heated and the temperature was controlled using a hot plate (IKA), with temperature controller (ETS-D5) and aluminium jacket to improve heat transfer. Liquid samples were collected using a stainless steel sampling tube equipped with a

ball valve. The outlet of the reactor is connected to a stainless steel condenser kept at -18 °C and 10 bar, to condense the volatile compounds back to the autoclave. Pressure was kept constant using a back pressure regulator (RHPS series dome-loaded pressure regulator by Proportion-Air Inc, with a 0-90 bar calibrated range). For this study, the autoclave was operated at 10 bar and variable temperature, 100-160 °C.

The reactor was equipped with three feeding gas lines (N_2; 10% O_2 in N_2; and a specified concentration of NO_x in N_2) operated through mass flow controllers (SmartTrack 100 Sierra), see Figure 1. Gas flow rates were adjusted to achieve the desired concentrations and the flows were pre-mixed before feeding them to the system through the tubing immersed into the liquid. The gas entering the reactor (a surrogate for the gas in the quench layer next to the engine cylinder wall) contained 95% N_2 and 5% O_2; the concentration of NO was varied between 0 and 500 *x*ppm, and that of NO_2 – between 0 and 100 *x*ppm. For all the experiments, the total gas flow rate was kept at 400 N-mL·min^{-1}, corresponding to 50-60 mL·min^{-1} at 10 bar and 100-160 °C. The head-space volume of the reactor is 90 mL.

A significant fraction of the gas phase in the autoclave is isooctane vapour – using the vapour pressure formula from Ref. [31], one obtains mole fraction of the isooctane in the gas phase of x_{C8} = 0.104, 0.177, 0.284, 0.353, and 0.433 at temperature T = 100, 120, 140, 150, and 160 °C, respectively (Table 1). Thus, 35.3% of the gas phase at 150 °C is isooctane vapour, which has to be accounted for when the gas phase concentrations are calculated – the concentration of component i in the autoclave is computed as $C_i = x_{i0}(1-x_{C8})p/RT$, where x_{i0} is the mole fraction of i in the gas phase before it is introduced in the autoclave, p is pressure, R is the gas constant (cf. supplementary information S1 for a list of symbols). Assuming Henry's constant (liquid concentration/gas concentration ratio) of $K_H^{CC} \approx 1$ for O_2 and NO_x in isooctane, and taking into account the amount of isooctane vapour in the gas phase, we can compute the mean residence time of NO_x and O_2 in the reactor as:

$$\tau = [V^L + (1-x_{C8})\times V^G] / F, \quad (1)$$

where V^L is the volume of the liquid isooctane (corrected for the thermal expansion), V^G is the volume of the remaining gas, and F is the flow rate in m^3·s^{-1}. This gives τ = 120 s at 160 °C and 170 s at 100 °C (Table 1). The decrease in τ with temperature is due to the increase in the vapour pressure of isooctane. Density of isooctane at each temperature was computed using the empirical formula from Ref. [32].

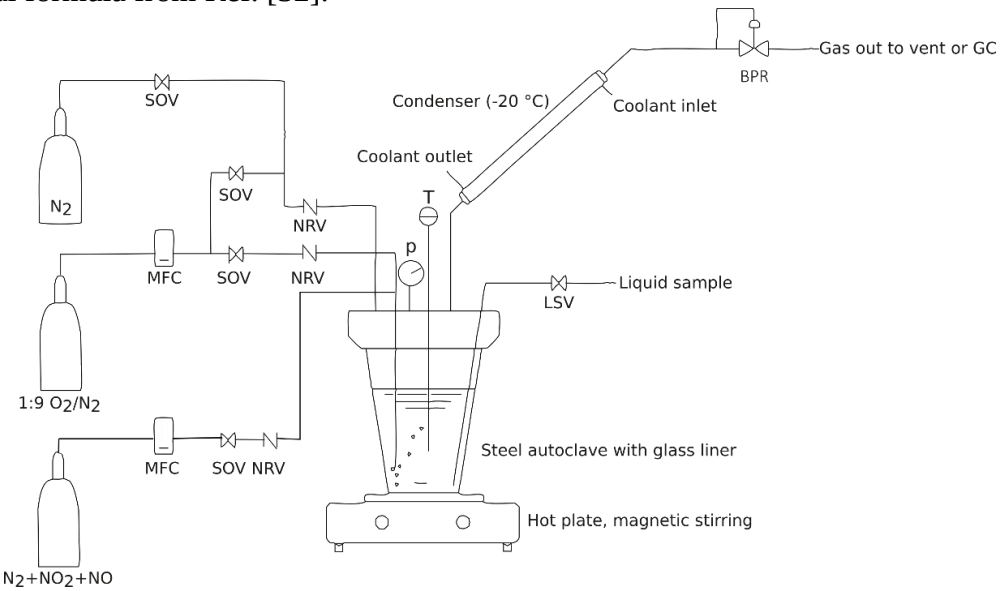

Figure 1. Scheme of the reactor.

Table 1. Conditions inside the reactor.

temperature T [°C]	25	100	120	140	150	160
[a] mole fraction of isooctane in the gas phase, x_{C8}		0.104	0.177	0.284	0.353	0.433
[b] density of liquid isooctane, ρ_{C8} [kg·m^{-3}]	689	622	601	577	564	551
[c] estimated residence time of NO_x, τ [s]		167	152	136	128	120
the CSTR concentration of NO_2 corresponds to feed concentration of NO_2 in $x$ppm of:		294	259	212	183	149

[a] Calculated using the theoretical isooctane vapour pressure formula from Ref. [31]. [b] Calculated using the empirical equation of state of liquid isooctane form Ref. [32]. [c] Computed using Eq (1). [d] Computed via Eq (5).

Experimental conditions studied. 60 mL of isooctane is loaded into the autoclave before sealing. Pure N_2 is fed to the head-space of the reactor until the desired pressure is reached and the initial temperature is established. The gas feed is then switched to a mixture of N_2, O_2, and NO_x through the bubbling line, of composition 5 x% O_2, 95 x% N_2 and specified trace amounts of NO_x. The start of the experiment is the start of the reactive gas flow. The experimental conditions adopted in this investigation, together with the abbreviations for the experimental runs, are summarized in Table 2.

Table 2. A list of conditions and labelling of the experiments.

Test	[NO_2] $x$ppm	[NO] $x$ppm	T °C	[TEMPO] $w$ppm
{O_2;T}	-	-	100-160 [a]	-
{O_2;T,Sc}	-	-	100-160 [a]	500
{NO_2;T}	100	-	100-160 [a]	-
{NO;T}	-	500	100-160 [a]	-
{NO_2;C}	5-100 [b]	-	150	-
{NO;C}	-	5-500 [b]	150	-
{NO_2+NO}	100		150	-
{NO_2+NO;Sc}	100		150	500

[a] Temperature was increased with time during these experiments, following the profile specified in Figure 3. [b] The concentration of NO_x was increased with time during these experiments, following the profile specified in Figure 7 in the S4.

The first two tests, {O_2;T} and {O_2;T,Sc}, were carried out without NO or NO_2. In the second test, {O_2;T,Sc}, a radical scavenger, 500 $w$ppm TEMPO, is present in the liquid phase. These experimental runs were devoted to checking the hypothesis that O_2 alone can produce significant oxidative degradation of isooctane under the conditions at the cylinder wall via direct hydrogen atom abstraction, according to the reaction RH + O_2 → R· + HO_2·. This process has often been assumed to be the key initiation reaction in autooxidation of fuels, e.g., Ref. [33]. Its rate at 160 °C is 4×10^{-9} M·s^{-1} (corresponding to 8×10^{-9} M·s^{-1} of radicals), according to Arrhenius's parameters from *table 4.1* in Ref. [34] and assuming Henry's constant $K_H^{CC} \approx 1$ for oxygen in isooctane. Such an initiation rate might produce detectable hydrocarbon degradation for lengths of the radical chain in the order of 100 or more. After the start of tests {O_2;T} and {O_2;T,Sc}, temperature was increased from 100 to 160 °C over 3-3.5 h in a stepwise manner, keeping it at 100, 120, 140, 150 and 160 °C, for ~30 min at each temperature; increasing the temperature from one value to another takes ~10 min (the temperature profile is plotted in Figure 3). Significantly, no products of degradation were detected, both in the presence and in the absence of TEMPO.

The next two tests, namely {NO_2;*T*} and {NO_2;*C*}, were performed in order to (i) find conditions at which the reactor can be operated safely with oxidation process having sufficiently high rate suitable for further investigation (oxidation rate $|d[O_2]/dt|$ of the order of 10-100 $mM \cdot h^{-1}$); (ii) identify the products of degradation of isooctane upon initiation by NO_2 but in the absence of NO. The feed concentration of NO_2 in the test {NO_2;*T*} was fixed at 100 *x*ppm, based on the estimation in Ref. [4] for the quench layer concentration at the cold injector wall; temperature was increased stepwise from 100 to 160 °C (as illustrated in Figure 3). The other test, {NO_2;*C*}, was performed at 150 °C (close to the typical gasoline injector wall temperature), while concentration of NO_2 was increased stepwise from 5 to 100 ppm over ~4 h (the time profile is specified in Figure 7 in S4).

Similarly, the tests {NO;*T*} and {NO;*C*} were performed in order to: (i) investigate to what extent can NO initiate a radical chain alone, in the absence of NO_2 in the feed gas, and (ii) find suitable conditions to study the degradation process while the reactor is operated safely. The temperature profile is unchanged compared to the tests {O_2;*T*} and {NO_2;*T*}; the concentration profile of {NO;*T*} corresponds to increasing the concentration from 10 to 500 ppm over ~4 h (Figure 7 in S4).

The next test, {NO_2+NO}, corresponds to a feed composition as closely resembling the conditions in the quench layer as possible with our set-up: 100 *x*ppm NO_2 and 500 *x*ppm NO, 150 °C, 10 bar [4]. The last test, {NO_2+NO;Sc}, corresponds to the same conditions but with added radical scavenger, TEMPO, in the liquid phase.

Detection and calibration. Identification and quantitative analyses of the products in the liquid phase were undertaken on an Agilent 7890GC integrated with a 5977 MSD and fitted with a CTC PAL autosampler. The GC-MS was equipped with a HP-InnoWax column (30 m × 0.250 mm × 0.25 µm). The identity of each compound was established using the NIST MS library and confirmed in some cases by injecting analytical standards. The samples were injected in the GC-MS without further dilution. Inlet temperature was 200 °C while the initial oven temperature was 35 °C, where it was held for 3 min, then ramped at rate 5 $K \cdot min^{-1}$ to 100°C, and subsequently to 200 °C at 20 $K \cdot min^{-1}$. Split ratio was 50:1 and total analysis time was 21 min. Liquid samples were collected at different experimental times and stored at 4 °C before analysis (performed immediately after the end of each run). The concentrations of acetone, methylpropan-2-ol (C4OH) and 2,4,4-trimethylpentan-2-ol ($C8_4OH$) were followed quantitatively using calibration curves (concentration vs. integrated signal area; linear regression was used for acetone and quadratic for the alcohols, st. dev. 0.36 mM for acetone, 1.8 mM for C4OH, 0.28 mM for $C8_4OH$); more details are given in S3. Three isomers of $C8_4OH$ were identified among the products: 2,2,4-trimethylpentan-1-ol ($C8_1OH$), 2,2,4-trimethylpentan-3-ol ($C8_3OH$), and 2,4,4-trimethylpentan-1-ol ($C8_5OH$, cf. Figure 2). We estimated their concentrations by assuming the same signal-to-concentration calibration curve as for the main product, $C8_4OH$.

Health and safety measures. The isooctane is flammable and we took measures to work at conditions outside its flammability limits based on data from Refs. [35-40], cf. the supplementary material S2. In addition, NO_2 and NO are toxic gases; NO_2 and NO sensors were used to detect possible leaks (details are given in supplementary material S3). The increased concentrations of NO and NO_2 in the presence of water can produce acids (HNO_2, HNO_3) that can damage the GC internals and the column. To avoid this, we conducted the {NO_2;*C*} and {NO;*C*} tests with a slow increase in NO_x concentration, always keeping it at the ppm level, and in the absence of water. We estimated that the maximum concentration of NO_x at which we operate is such that the pH of a water droplet accidentally introduced in the column cannot fall below 3.6 assuming Henry's constant for NO_x in water of K_H^{CC} ~10.

3. Results

Level of degradation with and without NO_x.

The two tests {O_2;*T*} and {O_2;*T*,Sc}, in which no nitrogen oxides were fed to the reactor, produced no observable amounts of oxidation products. In all other tests, {NO_2;*T*}, {NO_2;*C*}, {NO;*T*}, {NO;*C*}, {NO_2+NO}, and {NO_2+NO;Sc}, significant degradation of the isooctane was evident, and more than 70 separate chromatographic peaks have been detected. The concentrations of the three components we followed reached up to 25 mM for 2,4,4-trimethylpentan-2-ol, 16 mM for acetone, and 16 mM for methylpropan-2-ol (Figure 3). The levels of degradation after the end of these tests are of similar order of magnitude, and similar GC peaks appear (cf. the chromatogram comparison in Figure 11 in S3), with important exceptions that are discussed below.

Reaction chemistry.

To interpret our results for the composition of the products of nitro-oxidation of isooctane, we formulated a reaction mechanism of the process (based on the theory of low-temperature radical chain autooxidation [34,38]). The mechanism produces a set of key reactive intermediates which could be inferred from the structure of the identified products. For the sake of brevity, we present the mechanism first, and below our evidence is provided. A simplified reaction scheme of the oxidation mechanism of isooctane is shown in Figure 2. The *first step* is the abstraction of hydrogen (aH) from isooctane by RO_2·, RO·, or NO_2, which produces four isomers of isooctyl (2,2,4-trimethyl-x-pentyl), corresponding to the four distinct carbon atoms from which a H-atom can be abstracted (C_1, C_3, C_4 or C_5). Abstraction by the alkyl peroxy radical RO_2· is highly selective and is expected to produce mostly *tert*- and some *sec*-isooctyl (2,2,4-trimethyl-4-pentyl and 2,2,4-trimethyl-3-pentyl); the more reactive alkoxy radical RO· should produce all four isooctyl isomers in similar quantities [38]. Thus, if aH is dominated by RO_2·, the aH-C_4-route in Figure 2 will be significantly faster than the other three routes; in contrast, a RO·-dominated radical chain will produce the products of all four degradation routes.

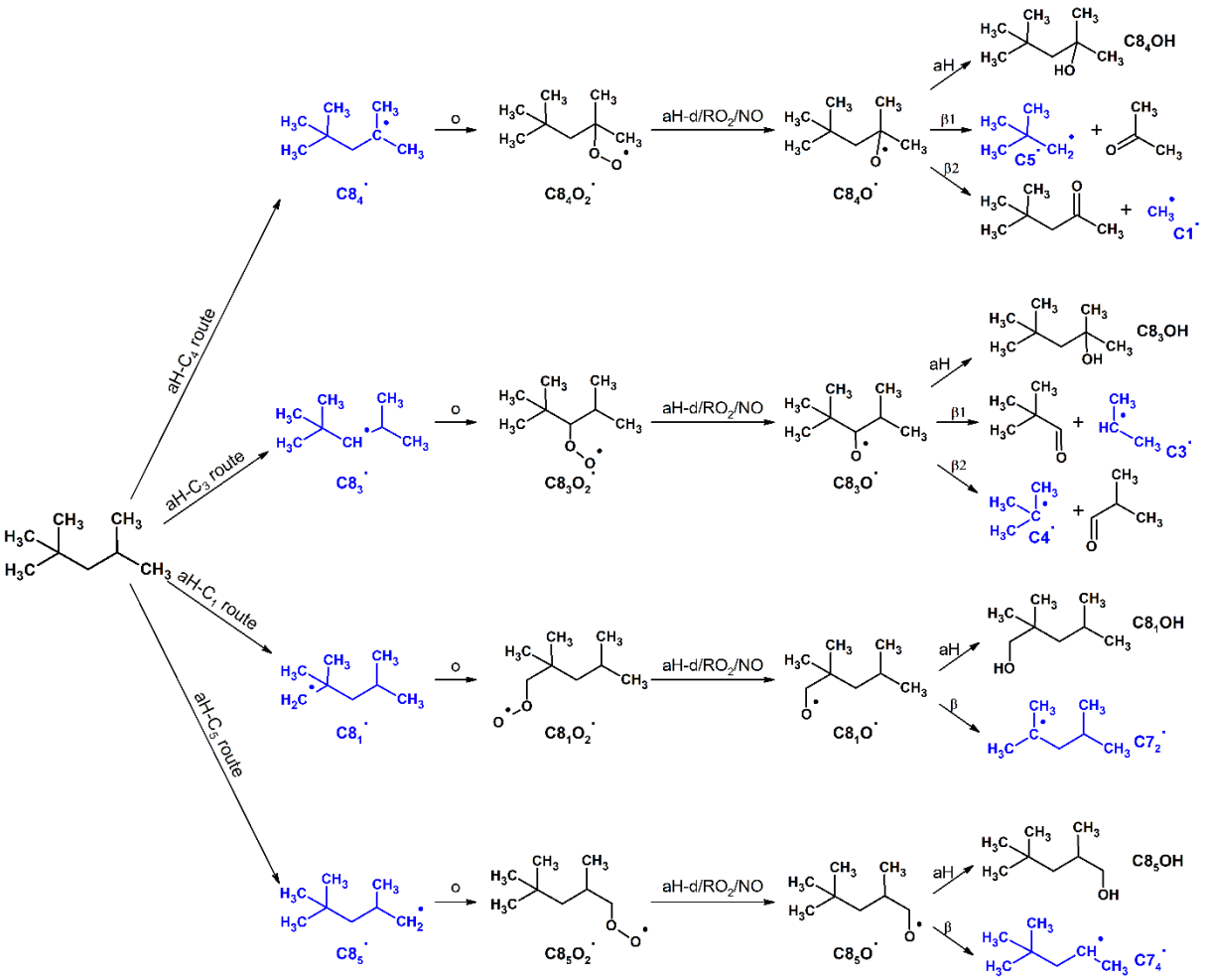

Figure 2. Reaction mechanism of isooctane and oxygen – key reactions. The key alkyl radicals formed are in blue.

The main *second step* is the oxidation (o) of the alkyls. It produces four alkyl peroxy radicals (isooctyl + O_2 → isooctylO_2·). These radicals are relatively stable and participate in a number of reactions: terminations with other radicals, inter- and intramolecular hydrogen abstraction and other rearrangements [34,38]. However, it seems that under the conditions at the wall of the cylinder, the main *third step* is the transformation of the alkyl peroxy radical to alkoxy radical via one of three possible routes [4,18,34,38,41]:

(i) reaction with NO: $RO_2\cdot + \cdot NO \rightarrow ROONO \rightarrow RO\cdot + \cdot NO_2$;

(ii) aH and decomposition: $RO_2\cdot \rightarrow RO_2H \rightarrow RO\cdot + HO\cdot$;

(iii) reaction with RO_2·: $2RO_2\cdot \rightarrow RO_4R \rightarrow 2RO\cdot + O_2$. (2)

In view of the high rate of the 1st reaction, we previously hypothesized that the rate-determining aH step of the radical chain will be dominated by RO· (aH is RO· + RH → ROH + R·) in the presence of NO, instead by the common RO_2·-dominated radical chains (aH is $RO_2\cdot$ + RH → RO_2H + R·) widely studied in the literature [33,34,38]. In the *fourth step*, the isooctoxy radicals (RO·) either abstract hydrogen atom from isooctane to produce the respective alcohols (which are the main primary products of the oxidation), or break to an alkyl radical and an aldehyde/ketone via a β-scission reaction.

According to the mechanism in Figure 2, a pool of 10 key alkyl radicals is present in the mixture:

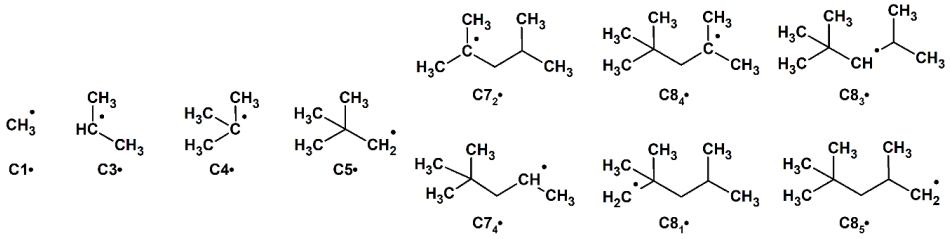

(3)

We use the following notation to denote these species: C1 (methyl), C3 (2-propyl), C4 (methyl-2-propyl), C5 (dimethyl-1-propyl), $C7_2$ (2,4-dimethyl-2-pentyl), $C7_4$ (4,4-dimethyl-2-pentyl), $C8_x$ (2,2,4-trimethyl-x-pentyl, where x = 1,3,4,5). All products that we were able to identify via GC-MS can be traced back to these radicals, or to their alkyl peroxy (RO_2·) or alkoxy (RO·) derivatives.

In the following, the main reactions and products are discussed.

Initiation.

The ability of NO_2 to abstract hydrogen from alkanes and initiate a radical chain oxidation is well-known, e.g., *sec. 3.3.2* of Ref. [34]; in contrast, NO is not known as a potent initiator. It is, therefore, not immediately clear what initiated the radical chain (i.e. abstracted hydrogen from isooctane) in tests {NO;*T*} and {NO;*C*}, where no NO_2 was fed to the autoclave. Time dependences of the experimentally determined concentration of 2,4,4-trimethylpentan-2-ol (which probably includes a fraction of the 2,4,4-trimethyl-2-hydroperoxypentane which is unstable and produces the alcohol) in tests {NO_2;*T*} and {NO;*T*} are compared in Figure 3a; as evident, the concentration profiles are similar. Since NO_2 is at 100 *x*ppm, while NO is at 500 *x*ppm, we can conclude that NO_2 produced 5-fold higher degradation rate than NO in these tests. Similarly, in the tests {NO;*C*} and {NO_2;*C*}, the first quantifiable amounts of acetone and 2,4,4-trimethylpentan-2-ol appeared at 20 *x*ppm of NO_2, while 5-fold higher concentration of NO (100 *x*ppm) is required for degradation products to be detected in {NO;*C*} (Figure 9 and Figure 7 in S4). The temperature in the tests {NO_2;*T*} and {NO;*T*} increases from 100 to 160 °C, yet concentration of 2,4,4-trimethylpentan-2-ol in Figure 3a follows a similar trend, which suggests also similar temperature dependence of the rate of production of this alcohol for the NO- and the NO_2-initiated processes.

These results can be explained with the oxidation of NO inside the autoclave in the reaction

$$2NO + O_2 \rightarrow 2NO_2. \quad (4)$$

This process can produce enough NO_2 to explain the observed degradation. The reaction follows the apparent rate law $r = k[NO]^2[O_2]$; the rate decreases with the rise in temperature, due to the slightly negative temperature dependence of k [42]. To estimate the resulting concentration of NO_2 in the reactor, we assume that the reaction (4) proceeds as if the involved reactants are in an ideal continuous-stirred tank reactor (CSTR). In this case, the mass balance of NO (neglecting the nitrogen oxides consumed by the autooxidation of the hydrocarbons) reads [43]:

$$\frac{[NO]_0 - [NO]}{\tau} = 2k[NO]^2[O_2], \quad (5)$$

where $[NO]_0$ is the initial concentration in the autoclave, after dilution with isooctane vapours, and τ is the mean residence time of NO in the gas (Table 1). Henry's constant of both [O2] and [NO] are assumed $K_H^{CC} \approx 1$.This quadratic equation determines [NO]; the produced amount of nitrogen dioxide is found from the mass balance $[NO_2] = [NO]_0 - [NO]$. Using the rate constant from Ref. [42], $k\,[M^{-2}s^{-1}] = 1200\times\exp(530/T[K])$, we find $[NO_2]$ that corresponds to a feed concentration 149 *x*ppm at 150 °C and 500 *x*ppm NO (after correcting for the isooctane vapours). Similar estimates are given in Table 1 for other temperatures and in Figure 7 in S4 for different $[NO]_0$. These numbers are providing an estimate of the upper limit for $[NO_2]$: in

the real reactor, the concentration of NO_2 in the bubbles right at the exit of the bubbling line will be close to zero while the one in the gas phase above the liquid isooctane should be closer to the CSTR value. The saturation of the liquid phase is likely to correspond to a NO_2 level in the middle between these two limits, i.e. roughly half the CSTR value. Thus, the quantity of NO_2 in tests {NO;*T*} and {NO_2;*T*} is of similar order of magnitude. The tests we did provided no evidence of direct hydrogen abstraction by NO (RH + NO → R· + HNO). For example, in {NO_2;*C*}, the 2,4,4-trimethyl-2-pentanol reaches concentrations above 1 mM only after the feed NO_2 level reached 50 *x*ppm; in {NO;*C*}, the same alcohol exceeded 1 mM after the feed NO level reached 200 *x*ppm, corresponding to 44 xppm NO_2, calculated through Eq. (5), cf. Figure 9 and Figure 7 in S4. This would not be the case if NO contributed significantly to the initiation.

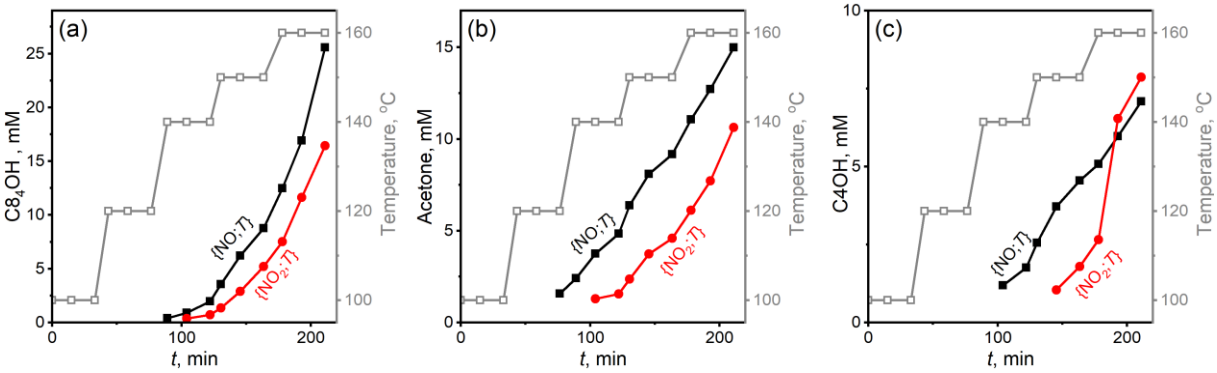

Figure 3. Time evolution of the concentrations in the liquid isooctane of (a) 2,4,4-trimethylpentan-2-ol, C8$_4$OH; (b) acetone; and (c) methylpropan-2-ol, C4OH. Comparison between tests {NO;*T*} (black squares) and {NO_2;*T*} (red circles). Temperature increases with time from 100 to 160 °C, following the same profile (open squares, right axis). Gas feed concentrations: $[NO]_0$ = 500 *x*ppm, $[NO_2]_0$ = 100 *x*ppm.

Hydroperoxides.

The alkyl radicals (3) react with oxygen to produce the corresponding alkyl peroxy radicals RO_2·, which can abstract hydrogen from isooctane to produce ten respective hydroperoxides RO_2H. Most of these are unstable under the conditions of the experiments and decompose via the reaction (2)-(ii). The three tertiary hydroperoxides are an exception: methylpropane-2-peroxol (C4O_2H); 2,4-dimethylpentane-2-peroxol (C7$_2O_2$H); and 2,4,4-trimethylpentane-2-peroxol (C8$_4O_2$H). C4O_2H was detected in significant quantities in all experiments; the chromatographic peaks of C7$_2O_2$H and C8$_4O_2$H could not be identified.

Alcohols.

The reactions (2) transform the alkyl peroxy radicals, RO_2·, to ten alkoxy radicals, RO·, that readily abstract hydrogen from isooctane to form the respective ten alcohols. All alcohols but the two most volatile have been detected: we could not identify the peaks of the methanol and 2-propanol in the liquid phase.

The primary isooctanols C8$_1$OH and C8$_5$OH are abundant in all runs in which NO was present in the gas phase. In comparison, their concentration was significantly lower in {NO_2;*T*} and {NO_2;*C*}. Similarly, the secondary isooctanol C8$_3$OH is of lower quantity in {NO_2;*T*} than in {NO;*T*}. At the same time, the amount of C8$_4$OH is similar, Figure 3a. To give an estimation of the amounts of C8$_x$OH, we assumed that the relationship signal-to-concentration from the calibration curve of C8$_4$OH is roughly applicable to the other three alcohols. This is probably not true – the isomers have vastly different retention times, to begin with ($\tau_{retention}$ = 9.3, 10.5, 14.6, 15.0 min for C8$_4$OH, C8$_3$OH, C8$_1$OH and C8$_5$OH, respectively); nevertheless, this approach allows a comparison between the different tests to be made. The concentrations obtained from the assumed calibration curves are plotted in Figure 10 in S4. After the end of

tests {NO;*T*}, the ratio of the three alcohols corresponds to selectivity ratios of approximately [$C8_4OH$]:[$C8_3OH$]/2 = 16 and [$C8_4OH$]:([$C8_1OH$] + [$C8_5OH$])/15 = 89 (i.e. the tertiary hydrogen is 16 times more reactive than the secondary, and 89 times more reactive than the primary). In {NO_2;*T*}, these are [$C8_4OH$]:[$C8_3OH$]/2 = 34 and [$C8_4OH$]:([$C8_1OH$] + [$C8_5OH$])/15 = 153, i.e. oxidation in the absence of NO is about twice as selective.

The selective production of the tertiary alcohol in the absence of NO is explained with the reaction (2)-(i): the nitric oxide produces RO· from RO_2·. Consequently, when NO is present, the hydrogen abstraction step of the radical chain propagation will transfer H from isooctane to the reactive non-selective RO·, while in the absence of NO, the hydrogen abstraction will proceed mostly through RO_2· and the tertiary C-H bond [38].

Aldehydes and acids.

Aldehydes can be produced either directly from the oxidation of the primary key radicals C1, C5, $C8_1$, and $C8_5$ (e.g., $RCH_2· + O_2 \rightarrow RCH_2O_2· \rightarrow RCH·O_2H \rightarrow RCHO + HO·$ [44]), or by β-scission of the alkoxy radicals C3, C5, $C7_4$, $C8_1$, $C8_3$, and $C8_5$ (as in the 4th step in Figure 2). Let us use for the first option the term C_1o-route, and for the second – the β-route. Most of the possible aldehyde products can be formed via one of these routes only; formaldehyde and dimethylpropanal can be formed via both:

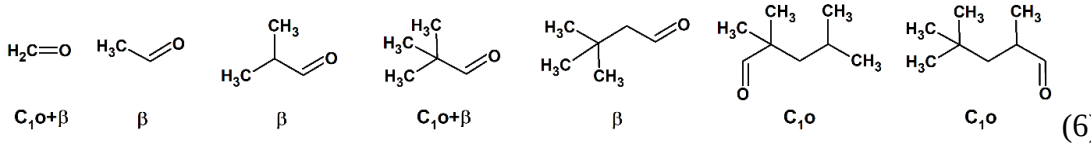

(6)

Dimethylpropanal is the only aldehyde we detected in the liquid phase. The probable reason for the absence of aldehydes is that they are easily oxidized to the respective acids [34,38]. Three of these acids were identified: methylpropionic, dimethylpropionic and 3,3-dimethylbutanoic, corresponding to the 3rd, the 4th and the 5th aldehyde in the list (6). Two major late peaks in the chromatograms might well be the two isooctanoic acids, but we could not ascertain that. Formic acid was not detected, but we identified small quantities of some esters of it with the alkanol products, including C4OCOH, C5OCOH and $C8_5$OCOH.

The evolution of the concentration of the acids is somewhat similar to that of methylpropan-2-ol in Figure 3(c). In the absence of NO (i.e. in tests {NO_2;*T*} and {NO_2;*C*}), the acids appear at an earlier stage compared to {NO;*T*} and {NO;*C*}. This can be explained with the low rate of route C_1o, because of the low concentration of primary radicals in RO_2·-dominated radical chain propagation in the absence of NO. The rate of the β-route is also higher in the presence of NO, as it starts with β-scission of RO· produced in reaction (2)-(i). However, the final concentrations of acids in {NO_2;*T*} and {NO_2;*C*} are significantly higher than in the presence of NO. A tentative explanation is that NO produces more acidic medium and catalyses secondary reactions depleting the acids, e.g., esterification.

Ketones.

Ketones can be produced also either by direct oxidation of the primary key radicals C3, $C7_4$, and $C8_3$ (e.g., via $R_1R_2CH· + O_2 \rightarrow R_1R_2CHO_2· \rightarrow R_1R_2C·O_2H \rightarrow R_1R_2CO + HO·$ [44], C_2o-route) or by β-scission of the alkoxy radicals C4O·, $C7_2O$·, and $C8_4O$· (as in Figure 2; β-route). A third possibility, the R_3O_2-route, is ketone production through intramolecular rearrangement with alkyl transfer of the peroxide radicals $C4O_2$·, $C7_2O_2$·, and $C8_4O_2$· [44], via the reactions $R_1R_2R_3CO_2· \rightarrow R_2R_3C·O_2R_1 \rightarrow R_2R_3C=O + ·OR_1$. Four ketone products are possible in theory:

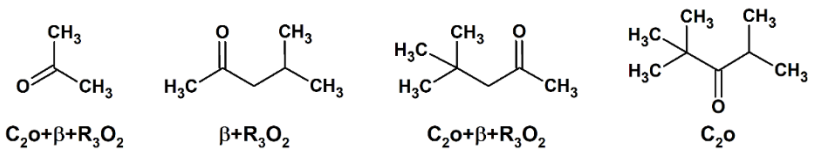

(7)

All but the second product (4-methyl-2-pentanone) were identified, and are present in all experiments in significant quantities.

Acetone is one of the main products of the oxidation. From Figure 3b, it can be concluded that acetone forms at higher *T* when NO_2 instead of NO is fed to the reactor, suggesting that the β-scission process that produces acetone (Figure 2) has a lower rate in the absence of NO. This is explained with the lower concentration of RO· radicals when NO is present, due to the process $RO_2· + NO \rightarrow RO· + NO_2$.

Radical isomerization.

Both the peroxide and the alkoxy radicals can undergo intramolecular radical abstraction reactions [34,38], producing 24 hydroperoxyalkyl (Figure 8 in S4) and 24 respective hydroxyalkyl radicals from the key alkyls (3). These 48 radicals produce a large number of polyfunctional compounds, most of which are hard to separate and identify. Only the following could be identified.

a) Diols and hydroxyalkanones. Two diols were detected. The 2,2,4-trimethylpentan-1,3-diol was produced in quantifiable quantities in the tests {NO;*T*}, {NO_2+NO}, and {NO_2+NO; *T*}, and its appearance is straightforward to explain, Figure 4b: a hydroperoxyalkyl or hydroxyalkyl is oxidized to alkyl dihydroperoxides, hydroperoxy alcohols and diols, following a process similar to those in Figure 2. The hydroperoxy groups then degrade to hydroxyl via Eq (2)-(ii). A much more significant product is, however, the 2,4-dimethylpentane-2,4-diol; for its production, there are at least 3 possible routes, shown in Figure 4a. It is likely that the process includes a step $RCH_2O· \rightarrow R·$, either by β-scission or via more complicated process. Both diols are of lower quantity in the absence of NO (cf. Table 3 in S3). This is due to the lower rate of formation of primary alkyl and hydroperoxyalkyl radicals in the absence of NO.

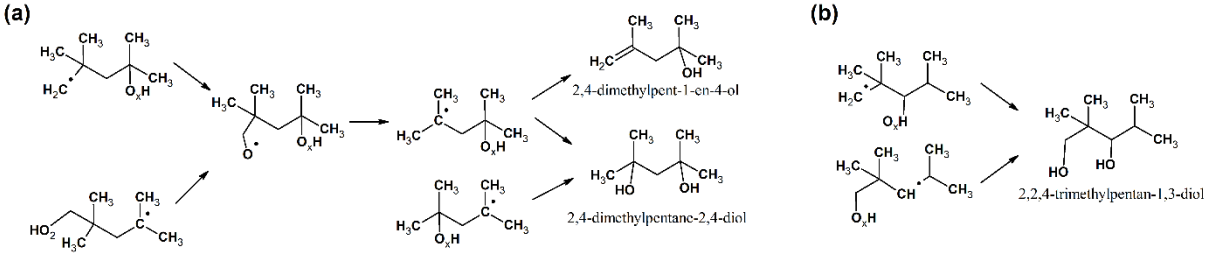

Figure 4. Mechanism of formation of the identified (a) diols, and (b) enol from the key hydroperoxyalkyls and hydroxyalkyls (cf. Figure 8 in S4). $–O_xH$ can be either –OH or $–O_2H$.

In addition, two hydroxyalkanones were detected: traces of 2,4-dimethyl-2-hydroxypentan-3-one, and 4-methyl-4-hydroxypentan-2-one, which has a significant peak in the chromatogram. Both compounds can be obtained via a great number of routes that resemble those in Figure 4. In addition, the 4-methyl-4-hydroxypentan-2-one might be a product of dimerization of acetone [45,46].

b) Alkenes. The β-hydroperoxyalkyl radicals decompose according to the reaction [44]:

$$>C·–C(O_2H)< \rightarrow >C=C< + HO_2·. \quad (8)$$

Eight different alkenes can be produced by this reaction: propene (from C3), methylpropene (from C4), several isomers of heptane, 2,4,4-trimethyl-1-pentene (from $C8_4$ and $C8_5$), and 2,4,4-trimethyl-2-pentene (from $C8_3$ and $C8_4$). Three of these products were detected – the methylpropene and the 2,4,4-trimethyl-x-pentenes. The alkenes are found in larger quantities

in the absence of NO (cf. Table 3 in S3). The reason is again the RO·-dominated chain in {NO;*T*} and {NO;*C*}: the reaction (8) is starting from peroxide radicals, and therefore its rate decreases when NO is present. The same type of reaction produces 2,4-dimethylpent-1-en-4-ol, cf. Figure 4a.

c) Heterocyclic products. The hydroperoxyalkyls are known to take part in cyclization reaction with release of HO· and formation of cyclic ethers [44]. Three products of this type have been identified:

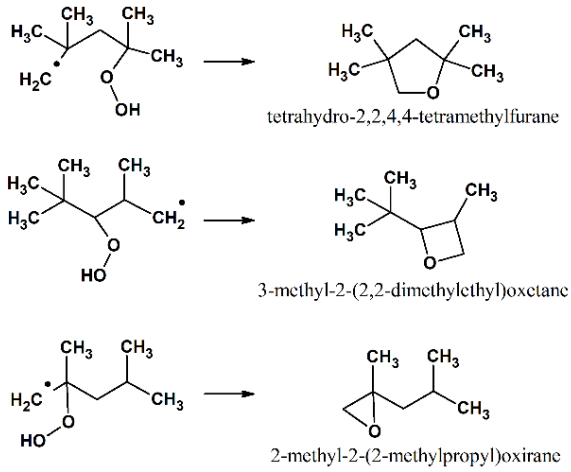

(9)

The tetrahydro-2,2,4,4-tetramethylfurane seems to be an important product producing a peak of a large area in the chromatogram. It is detected earlier and is of higher concentration in the absence of NO, which is explained with the need for a hydroperoxy group for the cyclization to take place. On the contrary, the 3-methyl-2-(2,2-dimethylethyl)oxetane is more concentrated in {NO;*T*} than in {NO_2;*T*}, probably because the formation of 2,2,4-trimethyl-3-hydroperoxy-5-pentyl is from the secondary 2,2,4-trimethyl-3-pentyl, which is more concentrated in {NO;*T*} than in {NO_2;*T*}, due to the selectivity of the hydrogen abstraction in the latter case. Small quantities of 2-methyl-2-(2-methylpropyl)oxirane were also detected in some experiments.

d) Other products and reaction routes. Small amounts of 4-methylpent-3-en-2-one were detected in test {NO_2+NO}, most probably as a result of the reaction (*p. 258* of [44]):

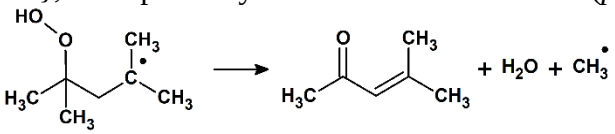

(10)

We detected traces of another conjugated carbonylalkene, (2,2-dimethyl)propylpropenal, in some of the experiments.

Nitrate esters and nitroalkanes.

A striking difference between nitro-oxidation with and without NO is that when the nitric oxide is present, it produces many organic nitrogen-containing compounds, while NO_2 alone does not, under the conditions of our experiments. Significant amounts of alkyl nitrates were detected, including the methylethyl- and the 3,3-dimethylpropyl esters of nitric acid ($C3ONO_2$ and $C5ONO_2$); none of these were detected in the absence of NO. The nitrates are probably produced by the process of isomerization of alkylperoxynitrite [18,41], via the scheme:

$$RO_2\cdot + \cdot NO \rightarrow ROONO \rightarrow RONO_2. \quad (11)$$

The formation of $RONO_2$ is rather important for the rate of the oxidation process, as it is a termination reaction, i.e. nitric oxide has an anti-oxidant radical scavenging effect. This is compensated to a large extend by the competing process $RO_2\cdot + \cdot NO \rightarrow ROONO \rightarrow$

RO· + ·NO_2, reaction (2)-(i), which produces reactive RO· that accelerate the hydrogen abstraction and, therefore, the rate of autooxidation [4].

In addition to nitrates, several nitro compounds have been identified; the 2,2,4-trimethyl-4-nitropentane ($C8_4NO_2$) was in quantifiable quantities whenever NO was present in the reactor, but was absent in tests {NO_2;*T*} and {NO_2;*C*}; traces of nitromethane and 2-methyl-2-nitropropane ($C1NO_2$ and $C4NO_2$) were also detected in {NO;*T*}. One bifunctional product, 1-nitromethylpropan-2-ol, has been detected, again only if NO is present in the reactor. The mechanism producing the nitroalkanes and the nitroalkanol is unclear.

Effect of the antioxidant. 500 *w*ppm of the radical scavenger TEMPO added to the isooctane results in approximately 2.5 times smaller amounts of oxidation products in test {NO_2+NO;Sc} compared to {NO_2+NO}, Figure 5. This means that the length of the radical chain in {NO_2+NO} is at least 3.5, i.e. every initiation event RH + ·NO_2 → R· + HNO_2 results in the production of at least 3.5 oxidized hydrocarbon molecules. TEMPO also has an effect on the selectivity of the reactions: the formation of acetone and especially *tert*-butanol is decelerated to a higher extent than the formation of the main product, $C8_4OH$. Surprisingly, *more* alkenes are produced when the antioxidant is present. The produced amounts of nitrates and nitrocompounds decrease only moderately or remain similar in the presence of the scavenger. The scavenger-produced change of selectivities relative to $C8_4OH$ are given in Table 3 in S3 for a list of products.

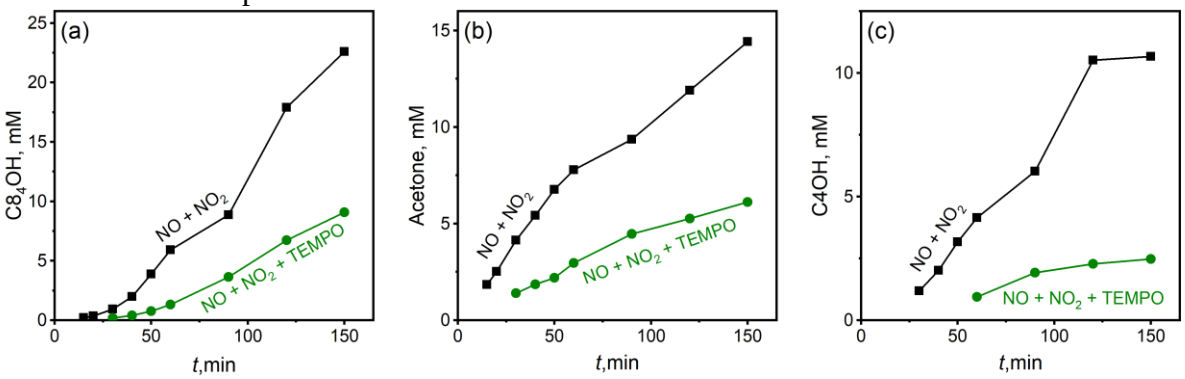

Figure 5. Effect of 500 *w*ppm radical scavenger TEMPO in the liquid isooctane on the evolution of the concentrations of (a) 2,4,4-trimethylpentan-2-ol; (b) acetone, and (c) methylpropan-2-ol; *T* = 150 °C, *p* = 10 bar, feed concentrations [NO_2] = 100 *x*ppm, [NO] = 500 *x*ppm, [O_2] = 5 *x*% (tests {NO_2+NO} and {NO_2+NO;Sc}, black squares and green circles respectively).

Reaction rates. This study was not designed as a kinetic study, so we leave the extraction of accurate rate law parameters for a future work. Yet, several important conclusions can be made based on the results.

As noted earlier [4], the rate of initiation due to the 5% O_2 present in the quench layer is negligible compared to the rate of initiation due to the reactive NO_2. However, the rate of the process *tert*-RH + NO_2 → *tert*-R· + HNO_2 that is predicted theoretically based on the parameters in *table 3.10* of Ref. [34] that we used previously [4] seems to be impossibly high. For example, in test {NO_2+NO}, where 100-280 *x*ppm of NO_2 are present, the theoretical initiation rate is $r_i = k[NO_2][\text{isooctane}] \approx 0.4\text{-}1.4$ mM·s^{-1}, using $k = 4.8$ M^{-1}s^{-1} based on Ref. [34]. The total rate of formation of 2,4,4-trimethylpentan-2-ol and acetone is 0.004 mM·s^{-1}, Figure 5; even if these main two products are only 10% of the total amount, this is still 0.04 mM·s^{-1} of oxidation products. Further, the radical chain length is at least 3.5, so a rough upper-limit estimate of the initiation rate would be 0.01 mM·s^{-1}, which is two orders of magnitude lower than the one predicted theoretically (i.e. the rate constant of *tert*-RH + NO_2 → *tert*-R· + HNO_2 at 150 °C is of the order of 5×10^{-2} M^{-1}s^{-1}).

Further, our study proves that the process $RO_2\cdot + \cdot NO \rightarrow RO\cdot + \cdot NO_2$ takes places at a significant rate under engine-relevant conditions. It produces RO·-dominated radical chain that results in a large number of different products in the presence of NO (primary and secondary alcohols, more aldehydes and acids, and low level of cyclic oxidized products and alkenes), as predicted in Ref. [4]. However, in contrast to the previous predictions, under the conditions of our test, this reaction does not accelerate the autooxidation process noticeably. This is likely due to the important radical scavenging reaction $RO_2\cdot + \cdot NO \rightarrow RONO_2$ that decelerates the autooxidation. In result, at least to the order of magnitude, we observe similar oxidation rates in all tests in which NO_x was fed to the autoclave.

Let us finally note that the liquid isooctane appears to be clear after all tests, and the degradation level is far from producing the characteristic yellow colour of degraded fuel, or phase-separated polar products (sludge).

4. Discussion and conclusion

In this work, we designed a test that allows the oxidative degradation of volatile hydrocarbons (components of gasoline) to be studied under conditions that are relevant to the engine cylinder walls and the crankcase, namely: high temperature and pressure, and presence of O_2, NO_2 and NO. We demonstrated the capabilities of the bench test by studying the oxidation of isooctane under various conditions. The major findings of the work are:

1. NO_2 initiates an oxidation radical chain process of a significant rate under the studied engine-relevant conditions. Oxygen alone, in the absence of NO_2, cannot produce observable rates of degradations, as predicted in Ref. [4] and proven by test {O_2;*T*}.

2. In confirmation of the prediction from our previous work [4] , via reaction (2)-(i), nitric oxide tends to produce alkoxy-dominated radical chain (hydrogen abstraction mostly by RO·), as opposed to a alkylperoxy-dominated one (hydrogen abstraction mostly by $RO_2\cdot$). This is proven by the NO-free tests {NO_2;*T*} and {NO_2;*C*}, in which we observed: (i) significantly lower relative concentration of primary and secondary alcohols, which are products of non-selective abstraction of hydrogen from isooctane typical for RO·; (ii) higher concentration of alkenes and tetrahydro-2,2,4,4-tetramethylfurane, which are typical products of $RO_2\cdot$ isomerization.

3. Nitric oxide produces a number of nitrogen-containing compounds that are absent if only NO_2 is fed to the reactor, among them alkyl nitrates and nitroalkanes. This suggests that an important radical scavenging reaction is taking place, $RO_2\cdot + NO \rightarrow RONO_2$, that decelerates the oxidation process. This compensates the acceleration due to the higher reactivity of RO· that dominates the hydrogen abstraction when NO is present. The overall result is that NO changes significantly the composition of the degradation products without changing drastically the oxidation rate.

4. In the absence of nitric oxide, NO_2 produces significant degradation even though no N-containing products have been detected. Under the conditions at the cylinder walls, NO_2 does not produce nitrates and nitroalkanes, in contrast with the reports in, e.g., Ref. [24]; NO does.

In the process of formation of gasoline injector nozzle deposits, the termination process (11) might be unimportant compared to (2)-(ii), as there the oxidation during the short cycle has been predicted to be in the accumulation stage [4], where the alkyl peroxy radicals $RO_2\cdot$ are of increasing (instead of steady-state) concentrations and the termination rate is still small. In the crankcase, the process (11) is most likely essential.

Another interesting finding is that NO produces significant amounts of NO_2 via reaction (4). This process is too slow to change the composition of the quench layer (the time of the engine cycle is ~50 ms, which is small compared to the characteristic time for oxidation of NO). However, this reaction will decrease the concentration of NO in the crankcase and in the lubricant, compare to Ref. [24].

The procedure and the bench test from this study can be used to study a number of other processes and cases important for deposition in gasoline engines, including: (i) study the role of the surface – steel vs. aluminium wall of the cylinder. (ii) Other gasoline components (alkenes, arenes); ethanolic gasoline; mixtures of lubricant + gasoline. (iii) Various additives of anti-oxidant action (radical scavengers, metal deactivators).

Acknowledgements. The funding and technical support from BP through the BP International Centre for Advanced Materials (BP-ICAM) made this research possible. The work was partly funded by the National Research Foundation (NRF), Prime Minister's Office, Singapore under its Campus for Research Excellence and Technological Enterprise (CREATE) programme. Markus Kraft gratefully acknowledges the support of the Alexander von Humboldt foundation.

References

1. Pearson R, Gold M, Filip S, Turner J, Stetsyuk V, Crua C, et al. Transient effects of fuel sprays on the surface wetting of diesel fuel injectors. Presented at the SAE International Powertrains, Fuels & Lubricants Meeting, Baltimore, Maryland, USA, 24-26 October 2016.
2. Eagle WE, Musculus MPB. Cinema-stereo imaging of fuel dribble after the end of injection in an optical heavy-duty diesel engine. THIESEL 2014 Conf Thermo-Fluid Dyn Process Direct Inject Engines 2014:1–20.
3. Imaoka Y. A study of particulate emission mechanism from injector tip deposit of direct-injection gasoline engines. Presented at the SAE International Powertrains, Fuels & Lubricants Meeting, Gasoline Direct Injection Deposits Workshop, Heidelberg, Germany, 20 September 2018.
4. Slavchov RI, Mosbach S, Kraft M, Pearson R, Filip SV. An adsorption-precipitation model for the formation of injector external deposits in internal combustion engines. Appl Energy 2018; 228:1423–38. https://doi.org/10.1016/j.apenergy.2018.06.130.
5. Aradi AA, Colucci WJ, Scull HM, Openshaw MJ. A study of fuel additives for direct injection gasoline (DIG) injector deposit control. SAE Tech. Paper 2000-01-2020. https://doi.org/10.4271/2000-01-2020.
6. Xu H, Wang C, Ma X, Sarangi AK, Weall A, Krueger-Venus J. Fuel injector deposits in direct-injection spark-ignition engines. Prog Energy Combust Sci 2015; 50:63–80. https://doi.org/10.1016/j.pecs.2015.02.002.
7. Dearn K, Xu J, Ding H, Xu H, Weall A, Kirkby P, et al. An investigation into the characteristics of DISI injector deposits using advanced analytical methods. SAE Int J Fuels Lubr 2014; 7:771–82. https://doi.org/10.4271/2014-01-2722.
8. Ariztegui J. Fast method of generating deposits in GDI engines and analysis of the impact on emissions. Presented at the SAE International Powertrains, Fuels & Lubricants Meeting, Gasoline Direct Injection Deposits Workshop, Heidelberg, Germany, 20 September 2018.

9. Harrison A, Cracknell RF, Krueger-Venus J, Sarkisov L. Branched versus linear alkane adsorption in carbonaceous slit pores. Adsorption 2014; 20:427–37. https://doi.org/10.1007/s10450-013-9589-1.
10. Liu X, Ito S, Wada Y. Oxidation characteristic and products of ETBE (ethyl tert-butyl ether). Energy 2015; 82:184–92. https://doi.org/10.1016/j.energy.2015.01.026.
11. Christensen E, Fioroni GM, Kim S, Fouts L, Gjersing E, Paton RS, et al. Experimental and theoretical study of oxidative stability of alkylated furans used as gasoline blend components. Fuel 2018; 212:576–85. https://doi.org/10.1016/j.fuel.2017.10.066.
12. Marie H, Deeg HP, Philipp H, Marukos N, Wang C. Study of interaction of N-methyl aniline octane booster on lubricating oil. SAE Tech Paper 2018-01–1809. https://doi.org/10.4271/2018-01-1809.
13. Marie H, Rigol S, Deeg HP, Philipp H. Impact of aniline octane booster on lubricating oil. SAE Tech Paper 2016:2016-01–2273. https://doi.org/10.4271/2018-01-1809.
14. Spindt RS, Wolfe CL, Stevens DR. Nitrogen oxides, combustion, and engine deposits. J Air Pollut Control Assoc 1956; 6:127–33. https://doi.org/10.1080/00966665.1956.10467741.
15. Dimitroff E, Moffitt J V, Quillian RD. Why, what and how: engine varnish. Trans ASME 1969; 91:406–16. https://doi.org/10.1115/1.3554951.
16. Hanson JB, Harris SW, West CT. Factors influencing lubricant performance in the sequence VE test. SAE International Fall Fuels & Lubricants Meeting and Exhibition, SAE International 1988; 881581. https://doi.org/https://doi.org/10.4271/881581.
17. Kuhn RR. *ACS Div Petrol Chem Petrol Preprints* 1973; 18:697–8.
18. Johnson MD, Korcek S. Effect of NOx on liquid phase oxidation and inhibition at elevated temperatures. Lubr Sci 1991; 3:95–118. https://doi.org/10.1002/ls.3010030203.
19. Johnson MD, Korcek S, Rokosz MJ. Effects of NOx on inhibition of oxidation by ZDTPS. *Lubr Sci* 1994; 6:247–66. https://doi.org/10.1002/ls.3010060304.
20. Murakami Y, Aihara H. Effect of NOx and unburned gasoline on low temperature sludge formation in engine oil. Int Congr Expo, SAE International 1991; 910747. https://doi.org/https://doi.org/10.4271/910747.
21. Miyata I, Hirano S, Tanada M, Fujimoto K. Mechanism of turbocharger coking in gasoline engines. SAE Tech Paper 2015-01-2029. https://doi.org/10.4271/2015-01-2029.
22. Jao T-C, Passut CA. Application of surfactants in lubricants and fuels. In: Zoller U, ed., Handbook of detergents, part E: applications. CRC Press, Taylor & Francis group, 2009; chapter 13, p. 331–44.
23. Colclough T. Lubricating oil oxidation and stabilisation. In: Scott G, ed., Atmospheric oxidation and antioxidants, vol. 2. Elsevier Science, 1993, chapter 1, p. 1–69. https://doi.org/10.1016/B978-0-444-89616-2.50005-7.
24. Lillywhite JRF, Sant P, Saville SB. Sludge formation: investigation of sludge formation in gasoline engines. Ind Lubr Tribol, 1990; 42:4-10. https://doi.org/10.1108/eb053400.
25. Nakamura K, Matsumoto E, Kurosaka S, Murakami Y. Effect of ventilation and lubricants on sludge formation in passenger car gasoline engines. SAE International Fall Fuels & Lubricants Meeting and Exhibition, SAE International 1988; 881577. https://doi.org/https://doi.org/10.4271/881577.
26. De la Cruz J, Estefan RM. Test apparatus and method for determining deposit formation characteristics of fuels. Patent 5,693,874, United States of America, 2 Dec 1997.
27. Kuprowicz NJ, Ervin JS, Zabarnick S. Modeling the liquid-phase oxidation of hydrocarbons over a range of temperatures and dissolved oxygen concentrations with

pseudo-detailed chemical kinetics. Fuel 2004; 83:1795–801. https://doi.org/10.1016/j.fuel.2004.03.013.
28. Kawamura M, Moritani H, Nakada M, Oohori M. Sludge formation and engine oil dispersancy evaluation with a laboratory scale sludge simulator. SAE International Fall Fuels & Lubricants Meeting and Exhibition, SAE International 1989; 892105. https://doi.org/https://doi.org/10.4271/892105.
29. Moritani H, Shimura Y, Mizutani Y, Hoshino K, Ueda F, Akiyama K. Investigation on oxidation stability of engine oils using laboratory scale simulator. SAE International Fall Fuels & Lubricants Meeting and Exhibition, SAE International 1995; 952528. https://doi.org/https://doi.org/10.4271/952528.
30. Aworinde SM, Wang K, Lapkin AA. Borate-assisted liquid-phase selective oxidation of *n*-pentane. Appl Catal A Gen 2018; 563:28–42. https://doi.org/10.1016/j.apcata.2018.06.023.
31. Slavchov RI, Novev JK, Mosbach S, Kraft M. Vapor pressure and heat of vaporization of molecules that associate in the gas phase. Ind Eng Chem Res 2018; 57:5722–31. https://doi.org/10.1021/acs.iecr.7b04241.
32. Pádua AAH, Fareleira JMNA, Calado JCG, Wakeham WA. Density and viscosity measurements of 2,2,4-trimethylpentane (isooctane) from 198 K to 348 K and up to 100 MPa. J Chem Eng Data 1996; 41:1488–94. https://doi.org/10.1021/je950191z.
33. Amara BA, Nicolle A, Alves-Fortunato M, Jeuland N. Toward predictive modelling of petroleum and biobased fuel stability: kinetics of methyl oleate/n-dodecane autooxidation. Energy and Fuels 2013; 27:6125–33. https://doi.org/10.1021/ef401360k.
34. Denisov ET, Afanas'ev IB. Oxidation and antioxidants in organic chemistry and biology, 1st ed. CRC Press, Taylor & Francis group, 2005.
35. Zabetakis MG, Scott GS, Jones GW. Limits of flammability of paraffin hydrocarbons in air. Ind Eng Chem 1951; 43:2120–4. https://doi.org/10.1021/ie50501a041.
36. Zabetakis MG. Flammability characteristics of combustible gases and vapors. Washington, US Dept of the interior, Bureau of Mines, 1965, bulletin 627.
37. Coward HF, Jones GW. Limits of flammability of gases and vapors. Washington, US Dept of the interior, Bureau of Mines, 1952, bulletin 503.
38. Bamford CH, Tipper CFH (editors). Comprehensive chemical kinetics: liquid-phase oxidation. Elsevier: Amsterdam, Netherlands, 1980.
39. Flasińska P, Fraczak M, Piotrowski T. Explosion hazard evaluation and determination of the explosion parameters for selected hydrocarbons C6-C8. Cent Eur J Energ Mater 2012; 9:399–410.
40. Setchkin NP. Self-ignition temperatures of combustible liquids. J Res Natl Bur Stand (1934) 1954; 53:49. https://doi.org/10.6028/jres.053.007.
41. Huie RE. The reaction kinetics of NO_2. Toxicology 1994; 89:193–216. https://doi.org/10.1016/0300-483X(94)90098-1.
42. Tsukahara H, Ishida T, Mayumi M. Gas-phase oxidation of nitric oxide: chemical kinetics and rate constant. Nitric Oxide - Biol Chem 1999; 3:191–8. https://doi.org/10.1006/niox.1999.0232.
43. Levenspiel O. Chemical reactor engineering, 3rd ed. John Wiley & Sons; 1999.
44. Fish A. Radical rearrangement in gas-phase oxidation and related processes. Q Rev Chem Soc 1964; 18:243–69. https://doi.org/10.1039/qr9641800243.
45. Chen C-I, Hsu SM. A chemical kinetics model to predict lubricant performance in a diesel engine. Part I: simulation methodology. Tribol Lett 2003; 14:83–90. https://doi.org/10.1023/A:1021748002697.

46. Diaby M, Sablier M, Le Negrate A, El Fassi M, Bocquet J. Understanding carbonaceous deposit formation resulting from engine oil degradation. Carbon 2009; 47:355–66. https://doi.org/10.1016/j.carbon.2008.10.014.

Supplementary information

S1. List of symbols and abbreviations

C_i	molar concentrations of *i* in the gas phase
F	feed volume rate
K_H^{CC}	Henry's constant, defined as ratio concentration in the liquid/concentration in the gas
k	rate constant
p	pressure in the autoclave
R	gas constant
r_i	initiation rate
T	temperature
t	time
V	volume of the autoclave
V^G	volume of the gas phase
V^L	volume of the liquid phase
x_{i0}	mole fraction of *i* in the gas phase before it is introduced in the autoclave
x_{C8}	mole fraction of the isooctane in the gas phase
ρ_{C8}	density of the liquid isooctane
τ	mean residence time
C1	methyl
C3	2-propyl
C4	methyl-2-propyl
C5	dimethyl-1-propyl
$C7_2$	2,4-dimethyl-2-pentyl
$C7_4$	4,4-dimethyl-2-pentyl
$C8_1$	2,2,4-trimethyl-1-pentyl
$C8_3$	2,2,4-trimethyl-3-pentyl
$C8_4$	2,4,4-trimethyl-2-pentyl
$C8_5$	2,4,4-trimethyl-1-pentyl
aH	abstraction of hydrogen by a radical
C_1o	oxidation of primary alkyls with formation of aldehydes
C_2o	oxidation of secondary alkyls with formation of ketones
o	oxidation of alkyl
R_3O_2	process of rearrangement of tertiary alkyl peroxy radicals with transfer of an alkyl group
β	β-scission process

{O_2;*T*}, {O_2;*T*,Sc}, {NO_2;*T*}, {NO_2;*C*}, {NO;*T*}, {NO;*C*}, {NO_2+NO}, {NO_2+NO;Sc}: codes to the eight experiments performed, as specified in Table 2. O_2 stands for "oxygen only", i.e. nitrogen oxides are absent. Sc stands for radical scavenger in the liquid phase. NO and NO_2 mean that these gases were present in the gas feed; note that NO_2 was present in the autoclave in {NO;*T*} and {NO;*C*}, due to the reaction (4), while no significant quantity of NO_2 is expected to appear in {NO_2;*T*} and {NO_2;*C*}. *T* stands for variable temperature; *C* stands for variable concentration of the NO_x during the experiment.

S2. Flammability limits and autoignition

Available data for the limits of flammability of isooctane as a function of the temperature *T*, at 1 atm, are summarized in the following table:

	x_{LL}, lower limit of flammability, 1 atm, *x*%	x_{UL}, upper limit of flammability, 1 atm, *x*%
26 °C	1.03 [a] [35]	
100 °C	0.96 [a] [35]	
150 °C	0.91 [a] [35]	
200 °C	0.88 [a] [35]	
60°C	0.77 [b]	6.1 [c]
100 °C	0.74 [b]	6.3 [c]
150 °C	0.71 [b]	6.5 [c]
200 °C	0.68 [b]	6.7 [c]
room temperature	0.98 [37]	6.03 [37]
24 °C	0.8 [39]	
60 °C		5.9 [39]

a. Extrapolation of the data from Ref. [35] to x_{LL} = 0 % gives 1200 °C for the flame temperature (close to the expected 1300 °C [36], confirming the reliability of the data). b. Extrapolated values under the assumption that the flame temperature is 1300 °C [36]. c. Extrapolated values using the modified Burgess-Wheeler law of Zabetakis, *eq 37* in Ref. [36], $x_{UL}/x_{UL,25\,°C}$ = 1+0.000721(T(°C)-25).

Further, we use the worst case scenario from the values in this table, namely x_{LL} = 0.8 % and x_{UL} = 6 % at room temperature, corresponding to 0.71 % and 6.5% at 150 °C, respectively, based on the correlations of Zabetakis [36].

We further correct these limits for the pressure dependence. To do so, we use the pressure dependence of natural gas (90% methane + 10% ethane) – its flammability limits depend on pressure as $x_{LL}/\% = 4.9 - 0.71\ \lg(p/\text{atm})$ for the lower limit and $14.1+20.4\ \lg(p/\text{atm})$ for the upper limit (fig 26 and eqs 41-42 in Ref. [36]). We assume that the pressure factor multiplying the ratio fuel/O_2 at the lower and the upper limits is similar for different fuels, given by

$$4.0757*(0.049-0.0030835*\ln(p/\text{atm}))/(.19971+0.0006475*\ln(p/\text{atm}))$$ and

$$1.27936*(0.141+0.088596*\ln(p/\text{atm}))/(0.18039-0.018605*\ln(p/\text{atm}))$$, respectively.

We multiply the upper and the lower limits of isooctane+air by these ratios, and then recalculate from them the respective x_{LL} and x_{UL} at the increased pressure. The pressure has little effect on the lower limit (0.58 % isooctane at 15 atm vs. 0.71 % at 1 atm, 150 °C), but it has a significant effect on the upper one (21% isooctane at 15 atm vs. 6.5 % at 1 atm, 150 °C).

We finally construct the flame stability diagram upon dilution with N_2 of isooctane + air. To do so, we use the fact that the diagram is close to triangular, the lower limit is nearly independent of the added N_2, and one of the edges of the triangle ("cusp") occurs near the stoichiometric mixture at the lower limit – this is illustrated in Figure 6.

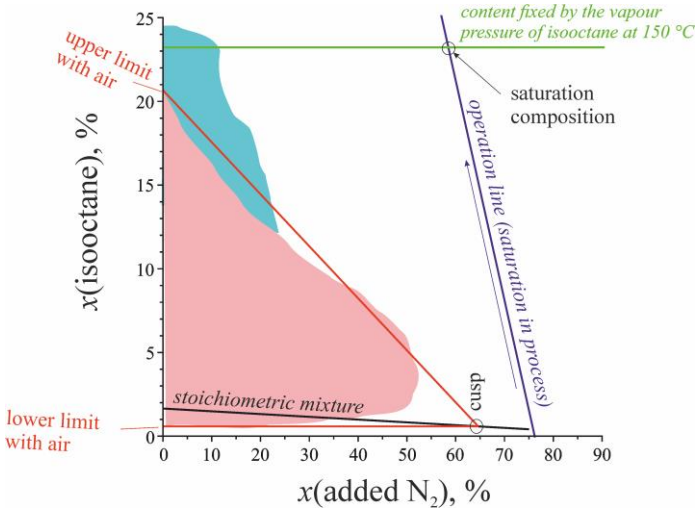

Figure 6. Flammability diagram for isooctane-nitrogen-oxygen mixtures – estimated flammability zone (red). Blue: rough estimation for the cool flame region. Green line: saturated isooctane vapour. Operation line: predicted conditions inside a gas bubble from entrance into the reactor (when *x*(isooctane) = 0) until saturation with isooctane vapour.

The real flammability zone is always covering a smaller area than the triangle, contained by the triangle (as schematically illustrated with the red zone). The cool flame zone is expected to be outside it – the blue shape in the figure – but no occurrence of cool flame should be expected at dilutions above 30%. The shapes of the coloured areas are based on those of various well-studied paraffins [36].

The vapour pressure of isooctane at 150 °C was calculated using the monomer-dimer Clausius formula from Ref. [31].We work with O_2:N_2 = 5:95. As the gas is bubbled through the isooctane, it will be diluted with isooctane vapours until it reaches saturation at 150 °C; this is not an instantaneous process, so the gas bubbles in the apparatus are expected to have all compositions from 0 to saturated concentration. These compositions correspond to the purple line in the figure (the operation line; the dilution of the N_2-O_2 mixture with isooctane vapours is taken into account). The gas composition, as seen, is expected to fall outside the flammability region under all conditions.

We also calculated the autoignition *T* of isooctane. At normal pressure, it is 683-720 K (Ref. [40] and others), and depends somewhat on the surface of the container. The autoignition *T* decreases with the increase in pressure. Judging from the data for 0.82 isooctane + 0.18 hexene (stoichiometric mixture, at 150 ms autoignition time), the increase in pressure leads to fall in the autoignition temperature by 5 $K \cdot atm^{-1}$ (in the range 10-13 bar), which is roughly 610-645 K at 15 bar; then, another extrapolation to autoignition time of 3 s (using Semenev's formula with activation energy of 110 $kJ \cdot mol^{-1}$) gives 550 K, or 277 °C. This is well above the studied temperature range. Another check of this estimate was done as follows: the autoignition temperature of isooctane (average chain length of 4.2) should be expected to be between those of butane (400 °C at increased pressure) and pentane (300 °C). The fact that we are not going to work with stoichiometric mixture is going to raise the autoignition temperature significantly.

S3. Toxicity of NO and NO_2

The immediately dangerous to life and health (IDLH) concentration (as specified by the National Institute for Occupational Safety and Health) of NO is 100 *x*ppm, and of NO_2 – 20 *x*ppm. The concentrations and the amounts of NO and NO_2 in the three cylinders were

chosen to be small enough that even the simultaneous discharge of all three cylinders in the laboratory space would result in concentrations well below IDLH. As an additional safety measure, we installed MultiRAE with sensors for NO and NO_2 to monitor for fast leak (faster than 50 $L \cdot min^{-1}$).

The experiments were conducted in a safety cabinet equipped with fume extractor to remove any gas/liquid vapour residues. Under the most severe experimental conditions, the concentrations of NO and NO_2 in the autoclave are 100 *x*ppm NO_2 + 500 *x*ppm NO in 130 mL autoclave. After each experiment, 25-30 L N_2 was blown through the autoclave to evacuate the NO_x safely.

S4. Additional experimental results

The temperature profile in those tests in which the temperature was variable is specified in Figure 3. The concentration profiles of NO_x for those tests in which these concentrations were variable is specified in Figure 7. In test {NO;*C*}, the feed concentration of NO corresponds to a specific CSTR concentration of NO2, cf. Eq (5); this is also given in the figure.

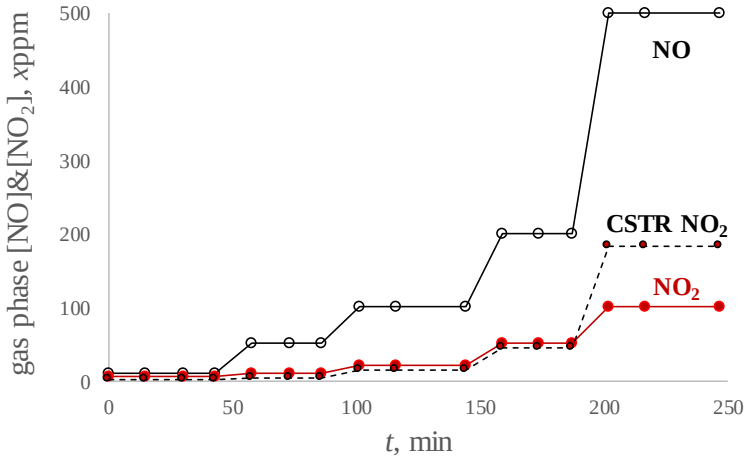

Figure 7. Concentration profiles in tests {NO_2;*C*} (red line) and {NO;*C*} (black lines). The points indicate where samples have been taken from the liquid phase for analysis. The plateau values for NO_2 correspond to 5, 10, 20, 50 and 100 *x*ppm; for NO, these are 10, 50, 100, 200, 500 *x*ppm. The dashed line "CSTR NO_2" is the estimated level of NO_2 in test {NO;*T*}, due to the oxidation reaction $2NO + O_2 \rightarrow 2NO_2$, cf. Eq. (5).

In Figure 8, we list all the perhydroxy alkyl radicals that can be produced from the key ten alkyl peroxy radicals $RO_2\cdot$, where R is one of the alkyls from the list (3). These are not of equal concentrations: the tertiary radicals are more stable, and those in which the H-O-O-C-…-C· sequence is 5 or 6 atoms long are more likely to appear [38]. There is a respective list for hydroxy alkyl radicals (that differ by a -OH instead of $-O_2H$ group); these are not as selective with respect to the tertiary position of the missing hydrogen atom, and those in which the H-O-C-…-C· sequence is 5 or 6 atoms long are more likely to appear [38]. However, the hydroxy alkyl radicals are thought to be more prone to β-scission reactions than to intramolecular hydrogen abstraction [44].

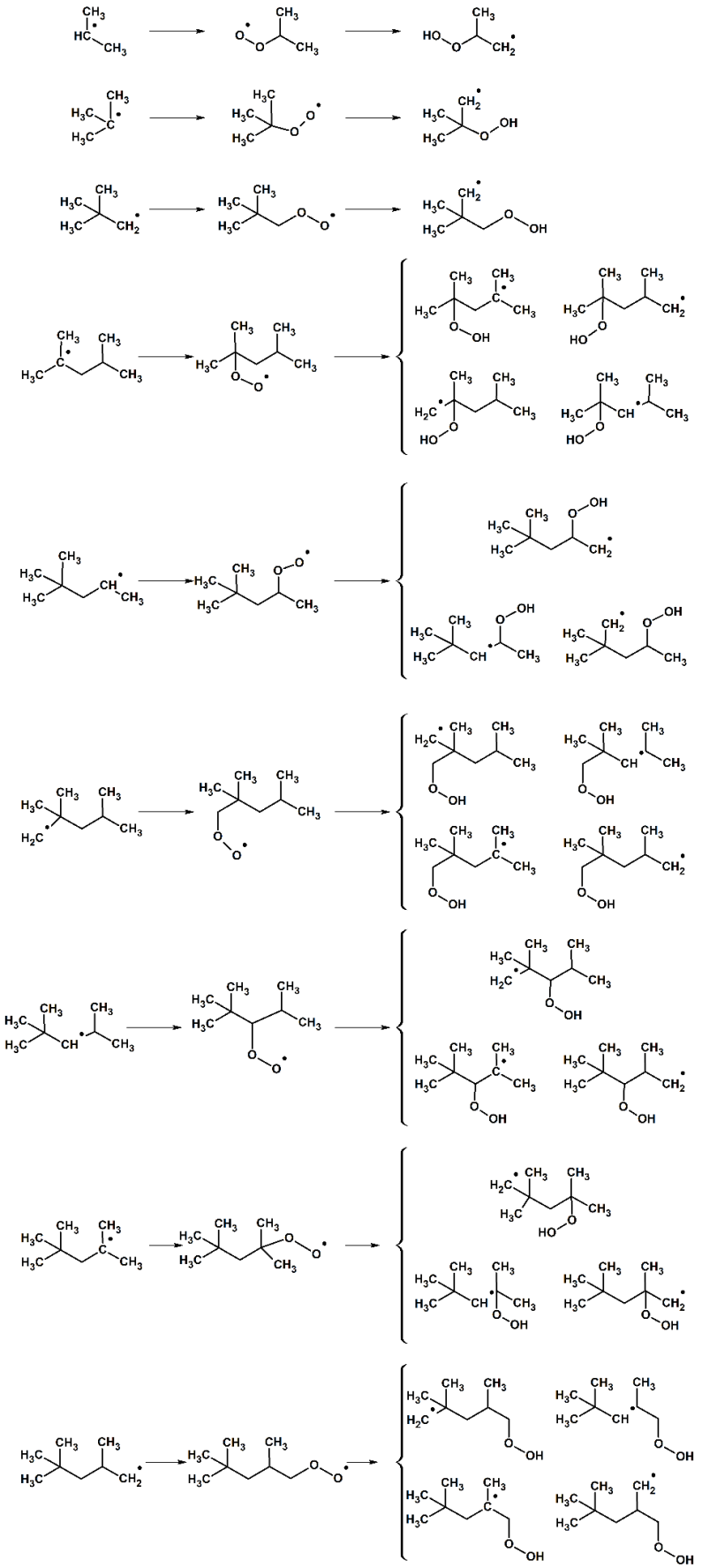

Figure 8. Key perhydroxy alkyl radicals produced by the nitro-oxidation of isooctane.

The concentrations of the three products that have been calibrated (acetone; 2,4,4-trimethylpentan-2-ol; methylpropan-2-ol) for tests {NO2;C} and {NO;C} are given in Figure 9. The concentrations of the four isomers of isooctanol ($C8_xOH$, x = 1,3,4,5) in tests {NO;*T*} and {NO_2;*T*} are given in Figure 10a; let us remind that only $C8_4OH$ has been calibrated, and for the other three alcohols the same calibration curve has been used, as a rough approximation. Similarly, the concentrations of $C8_xOH$ in tests {NO_2+NO} and {NO_2+NO;Sc} are plotted in Figure 10b.

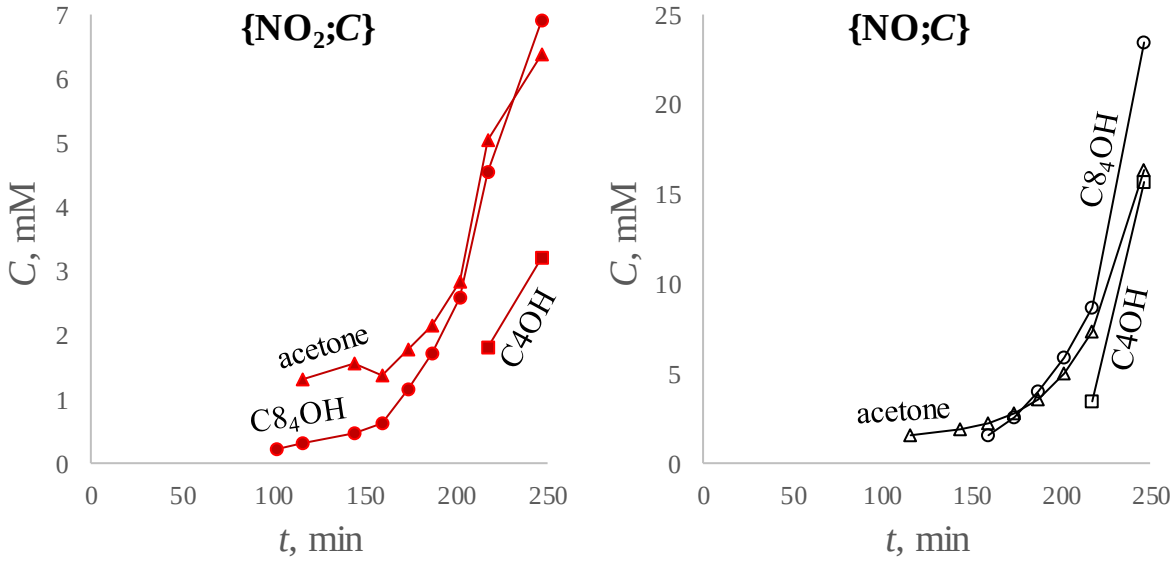

Figure 9. Evolution of the concentrations of 2,4,4-trimethylpentan-2-ol ($C8_4OH$), acetone, and methylpropan-2-ol (C4OH) in tests {NO_2;*C*} and {NO;*C*}.

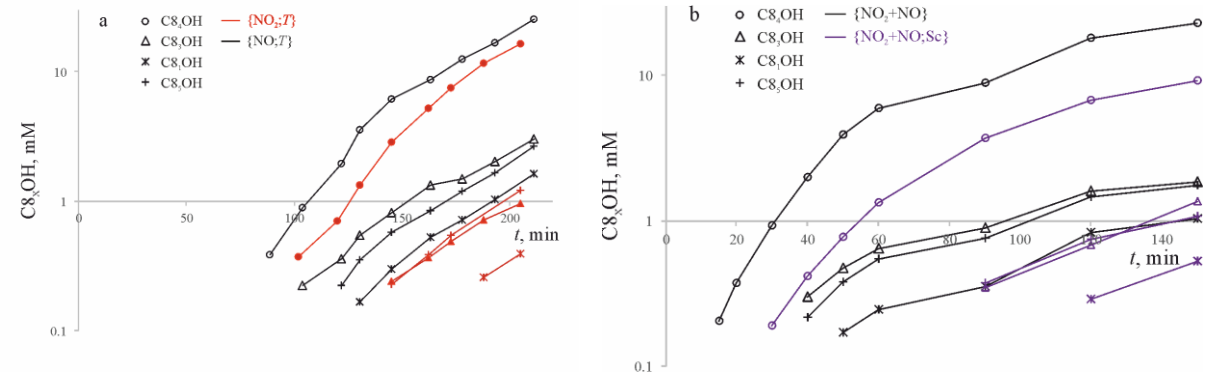

Figure 10. Concentration of the isomers of isooctanol ($C8_1OH$, $C8_3OH$, $C8_4OH$, $C8_5OH$) (a) in tests {NO_2;*T*} and {NO;T}; (b) in tests {NO_2+NO} and {NO_2+NO;Sc}. Only [$C8_4OH$] has been calibrated against the GC-MS signal – the other three concentrations are estimates only.

To compare the relative amounts of various products in tests {NO_2;*T*} than in {NO;*T*}, we used the values of the relative selectivity defined as:

$$S_i^T = \frac{area_i^{\{NO_2;T\}}}{area_i^{\{NO;T\}}} \times \frac{area_{C8_4OH}^{\{NO;T\}}}{area_{C8_4OH}^{\{NO_2;T\}}}. \quad (12)$$

Here, $area_i^{\{\ldots\}}$ stands for the area of the MS peak for compound *i* in test {…}, as determined in the last probe taken. A value of $S_i^T > 1$ means that a higher proportion of compound *i* is formed in {NO_2;*T*} than in {NO;*T*}, relative to $C8_4OH$, i.e. in the absence of NO *relatively* more *i* is produced. The selectivities S_i^C and S_i^{Sc} are similarly defined:

$$S_i^C = \frac{area_i^{\{NO_2;C\}}}{area_i^{\{NO;C\}}} \times \frac{area_{C8_4OH}^{\{NO;C\}}}{area_{C8_4OH}^{\{NO_2;C\}}}; \quad (13)$$

$$S_i^{Sc} = \frac{area_i^{\{NO_2+NO;Sc\}}}{area_i^{\{NO_2+NO\}}} \times \frac{area_{C8_4OH}^{\{NO_2+NO\}}}{area_{C8_4OH}^{\{NO_2+NO;Sc\}}}. \quad (14)$$

The values of the selectivities for several products are listed in Table 3. The selectivity shift in the presence of NO is also illustrated by the comparison of the chromatograms for tests {NO_2;*T*} and {NO;*T*} in Figure 11.

Table 3. Difference between the detected oxidation products in NO-nitro-oxidation and NO2-nitro-oxidation.

	[a] S_i^T {NO_2;*T*}:{NO;*T*}	[b] S_i^C {NO_2;*C*}:{NO;*C*}	[c] S_i^{Sc} {NO_2+NO;Sc}:{NO_2+NO}
$C8_4OH$	1	1	1
$C8_3OH$	0.48	0.8	1.5
$C8_1OH$	0.35	0	1.02
$C8_5OH$	0.67	1.19	1.24
acetone	0.97	1	0.84
tert-butanol, C4OH	1.51	0.62	0.52
2,4,4-trimethyl-1-pentene	1.07	2.03	2.06
2,4,4-trimethyl-2-pentene	1.44	2.18	3.38
2,2-dimethyl-1-propanol nitrate	<<1	[e]	>>1
2,2,4-trimethyl-4-nitropentane	<<1	[e]	1.23
2-nitro-*tert*-butanol	<<1	[e]	1.67
dimethylpropanal	[d] 1.49	[e]	<<1
2-methyl propionic acid	[d] 1.41	[d] 1.34	0.57
2,2-dimethylpropionic acid	[d] 1.59	[e]	1.74
3,3-dimethyl-butanoic acid	[d] 3.49	[d] 3.79	0.51
2,2,4-trimethyl-1,3-pentanediol	0	[e]	[e]
2,4-dimethyl-2,4-pentanediol	0.87	0.84	0.53
tetrahydro-2,2,4,4-tetramethylfurane	0.99	2.07	>>1
2-dimethylethyl-3-methyloxetane	0.82	<<1	0.83

[a] Eq (12); if $S_i^T > 1$, then more *i* is formed in {NO_2;*T*} than in {NO;*T*}, relative to $C8_4OH$. [b] Eq(13); if $S_i^C > 1$, then more *i* is formed in {NO_2;*C*} than in {NO;*C*}, relative to $C8_4OH$. [c] Eq (14); if $S_i^{Sc} > 1$, then more *i* is formed in {NO_2+NO;Sc} than in {NO_2+NO}, relative to $C8_4OH$. [d] These compounds have $S_i > 1$ close to the end of the respective two tests, but $S_i < 1$ before that (behaviour like C4OH in Figure 3c). [e] Signal(s) not strong enough to evaluate the selectivities.

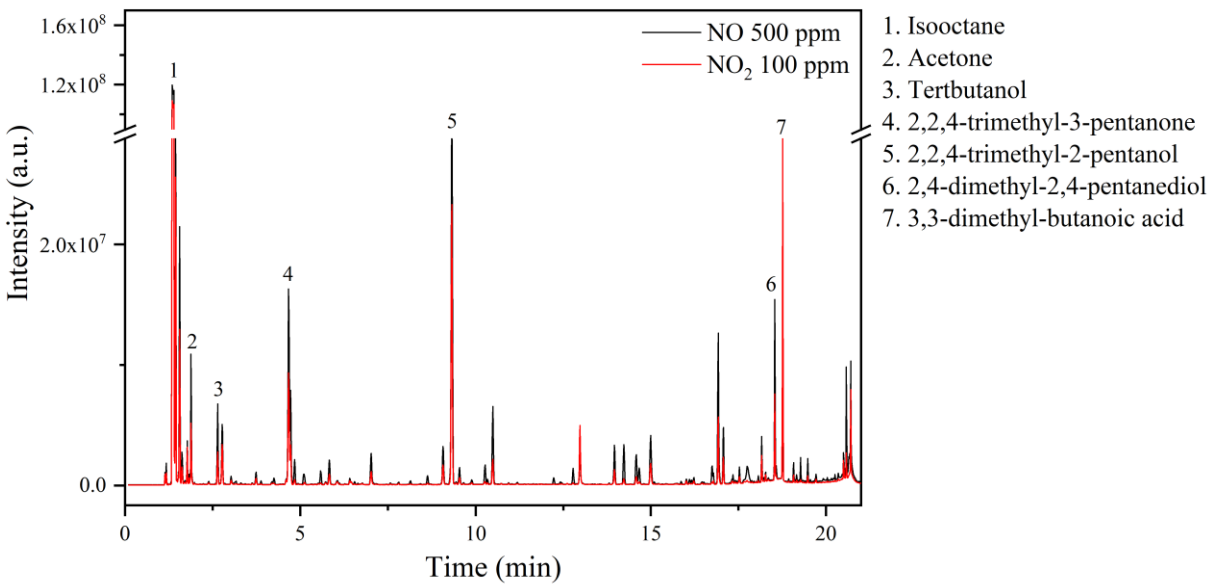

Figure 11. Chromatogram for nitro-oxidation of isooctane with 500 ppm NO or 100 ppm NO_2. Probes from tests {NO;*T*} and {NO_2;*T*}, respectively, taken 163 min after the start of the tests (33 min after 150 °C has been reached, cf. Figure 3).

Figure 12 is an example for the evolution with time and temperature of the chromatographic peak of one of the major products, $C8_4OH$, in test {NO_2;*T*}. No significant signal has been detected at temperatures lower than 140 °C. In all cases, no significant asymmetry of the peaks has been observed. The areas of the peaks were used to quantify the concentration of $C8_4OH$, Figure 3a, using a calibration curve (eleven solutions of $C8_4OH$ in isooctane, 6-50 mM).

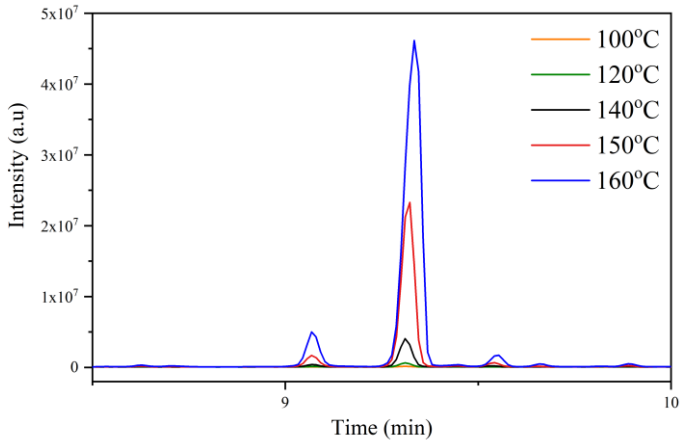

Figure 12. Evolution of the chromatographic peak of $C8_4OH$ with the advance of test {NO_2;*T*}; each curve corresponds to the GC-MS signal for the samples taken 30 min after the indicated temperature has been reached (cf. Figure 3 for the relation between time and temperature).